scientific reports

Check for updates

OPEN

Evaluating the diagnostic accuracy of ^{99m}Tc-labeled somatostatin receptor imaging for suspected pheochromocytomas and paragangliomas

Bo Li[1,5], Xintao Ding[2,3,5], Jie Zhang[1], Minmin Tang[1], Huimin Liu[4]✉, Xinyu Wu[1]✉ & Yongju Gao[1]✉

Pheochromocytomas and paragangliomas (PPGLs) present diagnostic challenges due to their diverse clinical manifestations. This study aims to evaluate the diagnostic accuracy of [^{99m}Tc]Tc-HYNIC-TOC SPECT/CT in patients with clinically suspected PPGLs. A retrospective analysis was conducted on 75 patients (36 males, 39 females, mean age 47.7 ± 14.9 years) with suspected PPGLs. All patients underwent [^{99m}Tc]Tc-HYNIC-TOC SPECT/CT imaging, and the results were compared with histopathological findings. The sensitivity, specificity, positive predictive value (PPV), negative predictive value (NPV), and overall accuracy of the imaging modality were calculated. Additionally, visual and semiquantitative evaluations were performed using Krenning score (KS) and tumor-to-background ratio (TBR), and their diagnostic performances were analyzed. Of the 75 patients, 54 had PPGLs (40 pheochromocytomas, 7 paragangliomas, and 7 metastatic PPGLs), and 21 had non-PPGL tumors. [^{99m}Tc]Tc-HYNIC-TOC SPECT/CT showed positive imaging in 63 patients, of whom 51 were confirmed as PPGLs and 12 as non-PPGLs. The sensitivity, specificity, PPV, NPV, and overall accuracy were 94.4% (51/54), 42.9% (9/21), 80.9% (51/63), 75.0% (9/12), and 80.0% (60/75), respectively. Visual and semiquantitative evaluations indicated higher KS and TBR values in PPGLs compared to non-PPGLs (median KS: 3.0 vs. 1.0, $P < 0.001$; median TBR: 2.10 vs. 0.92, $P < 0.001$). The Receiver operating characteristic (ROC) analysis revealed AUCs of 0.803 for KS and 0.791 for TBR, with no significant difference in their diagnostic performance ($P = 0.710$). Metastatic PPGLs were detected in 7 cases, with metastases observed in multiple organs. [^{99m}Tc]Tc-HYNIC-TOC SPECT/CT effectively diagnoses PPGL and identifies metastatic disease. Despite lacking comparative evaluation with established tracers, it represents a cost-effective alternative for PPGL evaluation, particularly in resource-limited settings where PET/CT access is restricted, bridging diagnostic gaps while maintaining acceptable accuracy.

Keywords [^{99m}Tc]Tc-HYNIC-TOC, SPECT/CT, Somatostatin receptor, Pheochromocytoma, Paraganglioma

Pheochromocytomas (PHEOs) and paragangliomas (PGLs), collectively termed PPGLs, are rare neuroendocrine tumors originating from chromaffin cells of the adrenal medulla and extra-adrenal paraganglia, respectively[1]. While these tumors are often distinguished by excessive catecholamine production, diagnosable biochemically with high sensitivity (99%), the specificity of these tests is lower (89%)[2]. Furthermore, some PPGLs are non-functional or present with non-specific clinical manifestations, posing significant diagnostic challenge[3]. Accurate diagnosis and localization are crucial for appropriate patient management and treatment planning.

[1]Department of Nuclear Medicine, Henan Key Laboratory of Novel Molecular Probes and Clinical Translation in Nuclear Medicine, Henan Provincial People's Hospital, Zhengzhou University People's Hospital, Henan University People's Hospital, Zhengzhou, China. [2]Department of Biomedical Informatics, Columbia University Graduate School of Arts and Sciences, New York, NY, USA. [3]Business & Strategy Analytics, Progyny, Inc, New York, NY, USA. [4]Department of Oncology, Henan Provincial People's Hospital, Zhengzhou University People's Hospital, Henan University People's Hospital, Zhengzhou, China. [5]Bo Li and Xintao Ding have contributed equally to this work. ✉email: hml0126@126.com; xinyu-wu2008@163.com; gyongju@hotmail.com

Conventional diagnostic techniques, such as computed tomography or magnetic resonance imaging, offer excellent morphological detail but often cannot reliably distinguish PPGLs from other adrenal masses or fully characterize multifocal disease, and lack functional information[4,5]. Consequently, functional imaging plays a pivotal role. Historically, [^{131}/^{123}I]I-Metaiodobenzylguanidine (MIBG) scintigraphy was a cornerstone for PPGL functional imaging due to its specificity for adrenergic tissue[6]. However, this technique has limitations, including restricted spatial resolution, difficulties in detecting small tumors (< 1.5–2.0 cm) or large tumors with extensive necrosis/bleeding, and potential drug interferences, which can lead to false-negative results[7]. According to current SNMMI/EANM guidelines, MIBG imaging is now primarily recommended for assessing MIBG avidity when considering [^{131}I]I-MIBG radiopharmaceutical therapy, rather than as a first-line diagnostic modality[8].

Recent genetic insights have shown that PPGLs are associated with various mutations influencing their behavior and imaging characteristics. The choice of functional imaging agent is increasingly guided by the underlying molecular profile of the PPGL. Somatostatin receptor (SSTR)-based imaging is particularly recommended for SDHx-related PPGLs (Cluster 1 A), which typically exhibit high SSTR expression[8]. Although [^{111}In]In-pentetreotide single photon emission computed tomography (SPECT) demonstrated superiority over MIBG in some PPGL evaluations, positron emission tomography (PET) with [^{68}Ga]Ga-labeled somatostatin analogues has gained popularity due to its superior resolution and quantitative advantages. This approach has proven highly sensitive and specific, often surpassing [$^{131/123}$I]I-MIBG imaging[9,10]. In contrast, [^{18}F]F-fluorodihydroxyphenylalanine ([^{18}F]F-FDOPA), which targets the L-type amino acid transporter 1 (LAT-1), is recommended as a preferred modality for PPGLs belonging to Cluster 1B, Cluster 2, as well as for sporadic tumors where SSTR expression may be less prominent[11–14].

In addition to PET-based SSTR tracers, [^{99m}Tc]Tc-labeled SSTR imaging agents, such as [^{99m}Tc]Tc-HYNIC-TOC, have garnered attention[15]. Given the lower costs of radiopharmaceuticals, the widespread availability of SPECT/CT equipment and reduced instrument installation expense compared to PET/CT systems, SPECT/CT holds promise for targeted SSTR imaging, especially in settings where PET/CT is not readily accessible[16]. However, to date, there have been very few reports on the clinical application of [^{99m}Tc]Tc-HYNIC-TOC in assessing the diverse spectrum of PPGLs, considering the molecular heterogeneity that influences optimal imaging strategies. To address this knowledge gap, we aim to present our findings on the diagnostic accuracy of [^{99m}Tc]Tc-HYNIC-TOC in a cohort of 75 patients with clinically suspected PPGLs.

Materials and methods

All the methods were performed in accordance with relevant guidelines and regulations.

Patients

This retrospective study analyzed 288 patients who presented with unexplained hypertension and had a high clinical suspicion of PPGL between November 2018 and April 2024. These patients were referred to the Department of Nuclear Medicine at Henan Provincial People's Hospital & Zhengzhou University People's Hospital for [^{99m}Tc]Tc-HYNIC-TOC SPECT/CT imaging to assess the possibility of PPGL. Patients with insufficient pathological data ($n = 154$) or incomplete follow-up information ($n = 59$) were excluded from the analysis. Ultimately, 75 patients met the inclusion criteria for the study. Demographic information were collected for each patient. The final diagnosis was confirmed through histopathological examination. PPGLs were categorized into adrenal PHEO or PGL. Metastatic PPGL was determined by the presence of metastasis to sites typically devoid of chromaffin cell tissue. The clinical characteristics of the patients are described in Table 1. This study was approved and waived by the Institutional Review Boards (IRB) of Henan Provincial People's Hospital & Zhengzhou University People's Hospital.

		PPGL	Non-PPGL	
Variable	**Overall, $N = 75$[1]**	**$N = 54$ (72%)[1]**	**$N = 21$ (28%)[1]**	**p-value[2]**
Age	47.68 (14.91)	47.41 (15.21)	48.38 (14.42)	0.797
Sex				> 0.999
Female	39 (52.00%)	28 (51.85%)	11 (52.38%)	
Male	36 (48.00%)	26 (48.15%)	10 (47.62%)	
Tumor size (cm)	4.10 [2.80, 5.60]	4.85 [3.43, 6.08]	2.70 [2.20, 4.20]	0.004
KS				< 0.001
0	12 (16.00%)	3 (5.56%)	9 (42.86%)	
1	9 (12.00%)	5 (9.26%)	4 (19.05%)	
2	19 (25.33%)	14 (25.93%	5 (23.81%)	
3	23 (30.67%)	21 (38.89%)	2 (9.52%)	
4	12 (16.00%)	11 (20.37%)	1 (4.76%)	
TBR	1.48 [0.93, 2.56]	2.10 [1.33, 3.43]	0.92 [0.73, 1.21]	< 0.001

Table 1. Patient characteristics. [1]Mean (SD); Median [IQR]; n (%). [2]Welch Two Sample t-test; Wilcoxon rank sum test; Pearson's Chi-squared test; Fisher's exact test. PPGL, pheochromocytomas and paragangliomas; KS, Krenning score; TBR, ratio between the maximal counts within the lesion and the mean counts within the liver.

[^{99m}Tc]Tc-HYNIC-TOC synthesis

The synthesis and labeling of [^{99m}Tc]Tc-HYNIC-TOC were performed according to previously established methods[17]. Briefly, a reaction mixture was prepared by combining 10 μg of HYNIC-TOC with 0.5 mL of EDDA (20 mg/ml in 0.1 M NaOH), 0.5 ml of Tricine (40 mg/ml in 0.2 M PBS, pH = 6.0), and 25 μl of $SnCl_2$ (1 mg/ml in 0.1 M HCl). Subsequently, 1110–2220 MBq of $Na^{99m}TcO4$ in approximately 1 mL of saline was added, and the mixture was heated at 100 °C for 20 min in a sealed vial. The solution was purified using a Sep-Pak mini cartridge (Waters, Milford, MA) eluted with 80% ethanol and diluted with 5 mL saline. The radiochemical purity, as determined by radio-thin-layer chromatography or high-performance liquid chromatography, was found to be not less than 95%.

[^{99m}Tc]Tc-HYNIC-TOC SPECT/CT acquisition and analysis

Images were acquired according to a previously published protocol and were performed using a hybrid SPECT/CT device (Discovery NM/CT 670, GE Healthcare, Haifa, Israel)[17,18]. Whole-body imaging was conducted 3–4 h post-intravenous administration of 555–740 MBq of [^{99m}Tc]Tc-HYNIC-TOC. A low-energy, high-resolution collimator with a 256 × 1024 matrix and a scan speed of 10 cm/min was used. SPECT/CT scans covering from the neck to the proximal thighs were acquired. The SPECT imaging parameters were a 6-degree angular resolution, 30 s per step, using a 256 × 256 matrix. CT scan parameters were as follows: 130 kV and 25 reference mAs modulation. CT data were reconstructed with a smooth (B41s) kernel at a slice thickness of 5 mm.

MEMRS-NM Workstation software (version 4.0.001, MedEx China Co., Ltd., Beijing, China) was employed for the analysis of SPECT/CT imaging. Two experienced nuclear medicine physicians, blinded to both the histopathological diagnosis and the interpretation of previously reported [^{99m}Tc]Tc-HYNIC-TOC imaging results, jointly interpreted the images. Lesions showing higher activity than adjacent normal tissues, unrelated to physiological uptake, were considered positive findings. Pathological uptake was assessed using the Krenning score (KS), a visual scoring system ranging from 0 to 4, with the liver and spleen as reference organs. The scores are defined as follows: 0 = uptake ≤ blood pool; 1 = uptake > blood pool but < physiologic liver uptake; 2 = uptake similar to physiologic liver uptake; 3 = uptake > physiologic liver uptake but < physiologic spleen uptake; 4 = uptake ≥ physiologic spleen uptake. To semi-quantitatively assess the pathological uptake of [^{99m}Tc]Tc-HYNIC-TOC, the tumor-to-background ratio (TBR) for each visually detected lesion was calculated as the quotient of the maximum counts within the lesion and the average counts within the liver.

Statistical analysis

Normally distributed continuous variables were expressed as mean ± standard deviation, while non-normally distributed variables were expressed as median (interquartile range). For normally distributed data, comparisons between two groups were conducted using the independent samples t-test, and comparisons among multiple groups were performed using one-way analysis of variance (ANOVA). For non-normally distributed data, the Mann-Whitney U test was used for comparison between two groups, and the Kruskal-Wallis H test was used for comparison among multiple groups. Frequency and percentage were used to describe categorical variables, and differences between groups were compared using the chi-square test or Fisher's exact test. The receiver operating characteristic (ROC) curves and Youden's J statistic were utilized to determine the optimal KS and TBR values for diagnosing PPGL. McNemar's test was used to compare the diagnostic accuracy of KS and TBR. Spearman's correlation coefficient was used to examine the correlation between the two variables. P value less than 0.05 was considered statistically significant. All statistical analyses were performed using R software (version 4.3.2).

Results

Patients' characteristics

Patient characteristics were depicted in Table 1. A retrospective analysis was conducted on 75 clinically suspected PPGL patients (36 males, 39 females). The age of the patients ranged from 15 to 75 years (mean age, 47.7 ± 14.9 years). The time interval between [^{99m}Tc]Tc-HYNIC-TOC SPECT/CT and histological results ranged from 1 to 3 weeks. Among the 75 patients, there were 54 cases of PPGL tumors and 21 cases of non-PPGL tumors. Of the 54 PPGL tumors, there were 40 cases of PHEO (including 4 cases of bilateral PHEO) (Fig. 1), 7 cases of PGL (Fig. 2), and 7 cases of metastatic PPGL. The most common pathological type of non-PPGL tumors was adrenocortical adenoma (AA), accounting for 16 cases (16/21, 76.2%). The remaining cases included 2 cases of adrenocortical carcinoma (AC), and one case each of neurofibroma (NF), G2 neuroendocrine tumor (NET), and high-grade serous carcinoma (HGSC). There were no statistically significant differences in age and gender between the PPGL and non-PPGL groups ($P = 0.797$ and $P > 0.999$, respectively), as shown in Table 1. However, there were significant statistical differences in tumor largest size, KS, and TBR between the two groups ($P = 0.004$, $P < 0.001$, $P < 0.001$), respectively.

The diagnostic accuracy of the [^{99m}Tc]Tc-HYNIC-TOC SPECT/CT

In this study, 63 showed positive [^{99m}Tc]Tc-HYNIC-TOC SPECT/CT imaging, while 12 exhibited negative results. Among the 63 patients with positive imaging, 51 were pathologically confirmed as PPGL tumors, and 12 were diagnosed with non-PPGL tumors (Fig. 3). For the remaining 12 patients with negative imaging, postoperative pathology revealed 9 cases of AA and 3 cases of PHEO. Therefore, the sensitivity, specificity, PPV, and NPV of [^{99m}Tc]Tc-HYNIC-TOC SPECT/CT for diagnosing PPGL were 94.4% (51/54), 42.9% (9/21), 80.9% (51/63), and 75.0% (9/12), respectively, with an overall accuracy of 80.0% (60/75) (Table 2).

Results of visual and semiquantitative evaluation

Of the 54 PPGL patients, 51 showed positive [^{99m}Tc]Tc-HYNIC-TOC SPECT/CT images, with varying uptake intensities ranging from weak to very strong. Among the 21 non-PPGL tumors, 12 exhibited positive uptake,

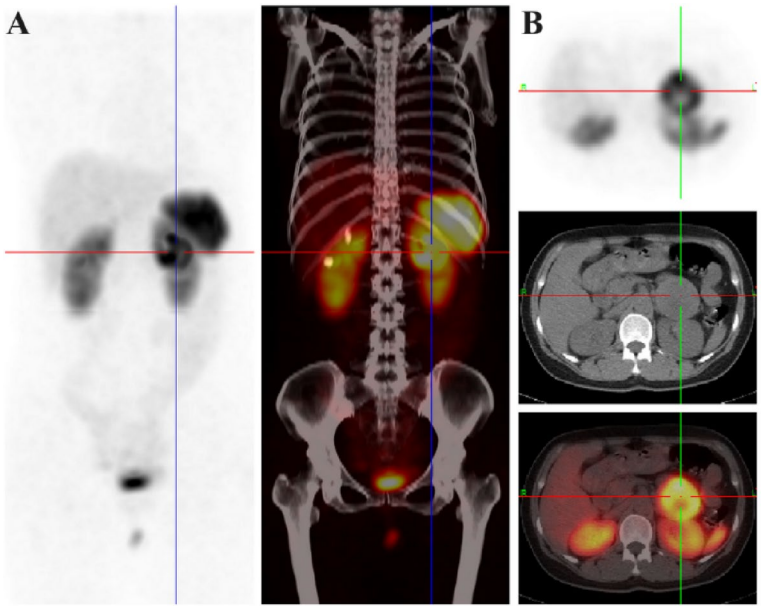

Fig. 1. A 38-year-old female presented with headaches and paroxysmal hypertension. CT revealed a mass in the left adrenal gland. [^{99m}Tc]Tc-HYNIC-TOC MIP image (**A**) shows an area of increased uptake of the radiotracer in the left adrenal region. The fused SPECT/CT image (**B**) demonstrates a left adrenal mass with a maximum diameter of 5.5 cm. The mass exhibits significant uptake of [^{99m}Tc]Tc-HYNIC-TOC, with a KS of 4 and a TBR of 7.07. The patient underwent surgery, and the diagnosis of pheochromocytoma was confirmed.

but with relatively weak to moderate intensities. The median KS in the PPGL group was significantly higher than that in the non-PPGL group (3.0 vs. 1.0, $P < 0.001$). Semi-quantitative analysis revealed that the median TBR in the PPGL group was significantly higher than that in the non-PPGL group (2.10 vs. 0.92, $P < 0.001$) (Table 1).

We performed a general ROC analysis including all PPGLs. The area under the curve (AUC) for KS was 0.803 (95% CI: 0.688–0.917), with optimal cutoff values of 2 (Fig. 4A). KS correctly diagnosed 46 PPGLs and 13 non-PPGL tumors, yielding sensitivity, specificity, PPV, NPV, and accuracy of 85.2% (46/54), 61.9% (13/21), 85.2% (46/54), 61.9% (13/21), and 78.7% (59/75), respectively (Table 3). The AUC for TBR was 0.791 (95% CI: 0.679–0.902) (Fig. 4B), with an optimal cutoff value of 1.356. TBR correctly diagnosed 40 PPGLs and 17 non-PPGL tumors, with sensitivity, specificity, PPV, NPV, and accuracy of 74.1% (40/54), 81.0% (17/21), 90.9% (40/44), 54.8% (17/31), and 76.0% (57/75), respectively (Table 3). McNemar's test showed no significant difference in diagnostic performance between the two methods ($P = 0.710$).

Correlation of tumor size with KS and TBR

We investigated the association between lesion size and respective visual and semi-quantitative parameters to ascertain whether tumor size correlates with SSTR expression. The mean tumor size was 4.8 ± 2.9 cm (median 4.1, range 0.9–13.7). Both KS and TBR showed moderate positive correlations with tumor size, with Spearman's correlation coefficients of 0.441 and 0.456, respectively (both $P < 0.001$) (Fig. 5).

Comparison between PHEO and PGL

The PHEO group comprised 46 patients, while the PGL group comprised 8 patients. There were no significant differences in clinical characteristics (gender and age) between the two groups (Table 4). The mean tumor size in the PHEO group was 5.4 ± 3.1 cm (median 4.8, range 0.9–13.7), which was slightly larger than that in the PGL group, with an average of 5.1 ± 2.2 cm (median 5.1, range 1.1–9.2), but there was no significant statistical difference between them. Additionally, we compared the KS and TBR values between the two groups, and the results indicated no statistical difference (P values were 0.491 and 0.141, respectively).

Metastatic PPGLs

A total of 7 patients were confirmed to have metastatic PPGLs. The diagnostic ability of [^{99m}Tc]Tc-HYNIC-TOC SPECT/CT to identify patients with metastatic disease was evaluated at the patient level. [^{99m}Tc]Tc-HYNIC-TOC SPECT/CT demonstrated positive findings consistent with metastatic involvement in all 7 of these patients, corresponding to a 100% patient-level detection rate for metastatic disease in this subgroup.

The observed metastatic sites included the lungs ($n = 6$), bones ($n = 4$), lymph nodes ($n = 2$), and liver ($n = 1$). Five of these patients presented with metastases in multiple sites. A statistically significant difference was observed in gender distribution between patients with non-metastatic and metastatic PPGLs ($P = 0.047$) (Table 4). The mean primary tumor size in patients with metastatic PPGLs was larger than in those with non-metastatic PPGLs (7.9 ± 4.4 cm vs. 4.9 ± 2.5 cm, respectively), although this difference did not reach statistical significance

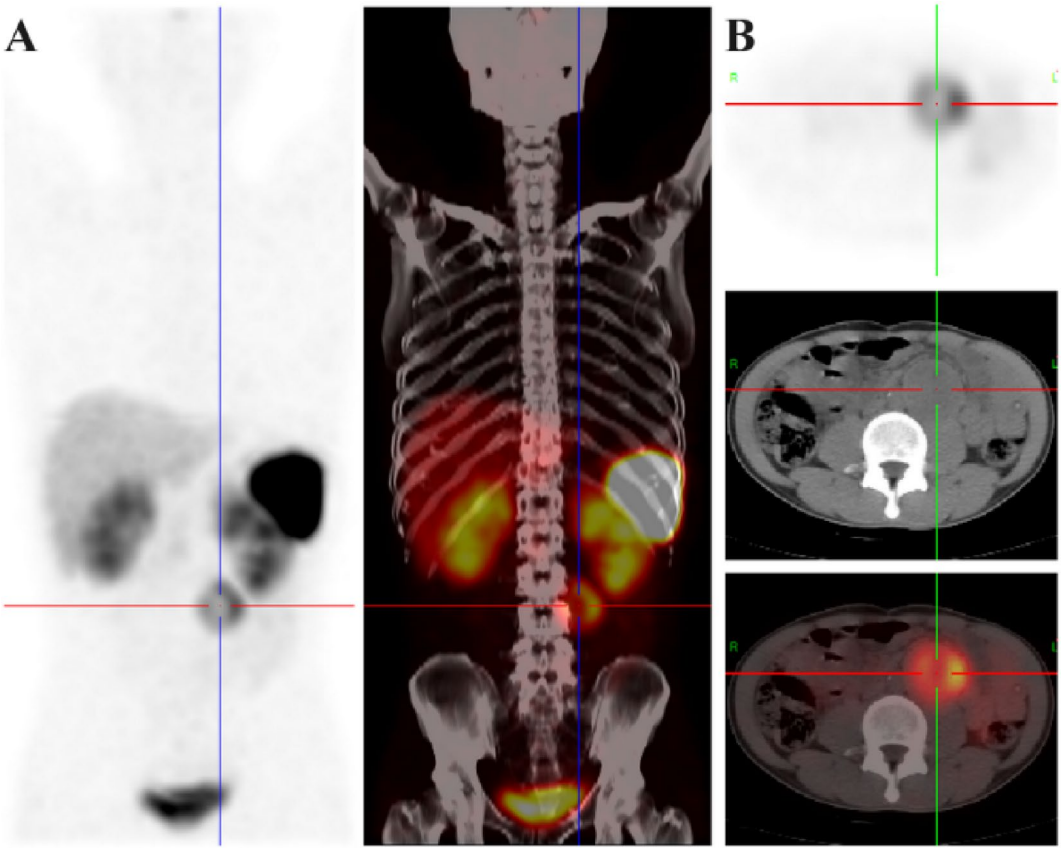

Fig. 2. A 27-year-old male with uncontrolled hypertension. [^{99m}Tc]Tc-HYNIC-TOC MIP image (**A**) demonstrates an area of abnormally increased radiotracer uptake in the left retroperitoneal region. SPECT/CT fused image (**B**) reveals a left retroperitoneal mass with a maximum diameter of 5.3 cm. The mass shows uptake of [^{99m}Tc]Tc-HYNIC-TOC, with a KS of 3 and a TBR of 3.00. The patient underwent surgery and was diagnosed with paraganglioma.

($P = 0.058$). Furthermore, comparison of KS and TBR values between the non-metastatic and metastatic groups revealed no statistically significant differences ($P = 0.750$ and $P = 0.562$, respectively).

Discussion

Accurate diagnosis and localization of PPGLs is essential for effective patient management and treatment planning. However, these tumors often exhibit non-specific clinical presentations and can manifest at diverse anatomical sites, thus posing significant diagnostic challenges. Although MIBG scintigraphy has traditionally been used, its utility is compromised by several limitations. The high expression of SSTR in PPGLs facilitates the detection of these tumors using SSTR-targeted imaging. To the best of our knowledge, there has been no systematic study in the literature regarding the use of [^{99m}Tc]Tc-HYNIC-TOC SPECT/CT for the detection of PPGLs. The present study addresses this gap by evaluating the diagnostic accuracy of [^{99m}Tc]Tc-HYNIC-TOC SPECT/CT in a cohort of 75 suspected PPGL patients. In our study, [^{99m}Tc]Tc-HYNIC-TOC SPECT/CT was evaluated as a diagnostic tool for PPGLs imaging. Our findings indicate that [^{99m}Tc]Tc-HYNIC-TOC SPECT/CT exhibits a high diagnostic performance for PPGLs on a per-patient basis, with a sensitivity of 94.4% (51/54), a specificity of 42.9% (9/21), and an accuracy of 80.0% (60/75).

For decades, several studies have indicated that [^{111}In]In-labeled octreotide imaging can be utilized for the detection of PPGLs[19,20]. One pioneering study reported an overall sensitivity of 22.0% in 53 PHEO patients, which is significantly lower than the sensitivity of 94.4% found in our study[19]. In a study by King et al.[20], the lesion detection rate was also lower, at 64.0%. These differences may be partly attributed to the differential tumor uptake of the imaging agents. Decristoforo et al. demonstrated that [^{99m}Tc]Tc-HYNIC-TOC has a higher affinity for SSTR binding compared to [^{111}In] In-pentetreotide[21]. The specificity of 42.9% in our study is relatively low, primarily due to the SSTR expression in non-PPGL lesions, such as adrenocortical adenomas[22]. These lesions accumulate radiotracers, mimicking PPGLs on imaging and challenging accurate differentiation based solely on tracer uptake. Analysis of false-positive cases revealed that 12 of 21 non-PPGL tumors showed positive uptake, predominantly with weaker intensities than PPGLs. Implementing optimized cutoff values substantially improved specificity: KS ≥ 2 increased specificity to 61.9%, while TBR ≥ 1.356 achieved 81.0% specificity, with corresponding sensitivity reductions to 85.2% and 74.1%, respectively. To enhance diagnostic accuracy, a multimodal approach incorporating biochemical markers (such as plasma free or urinary fractionated

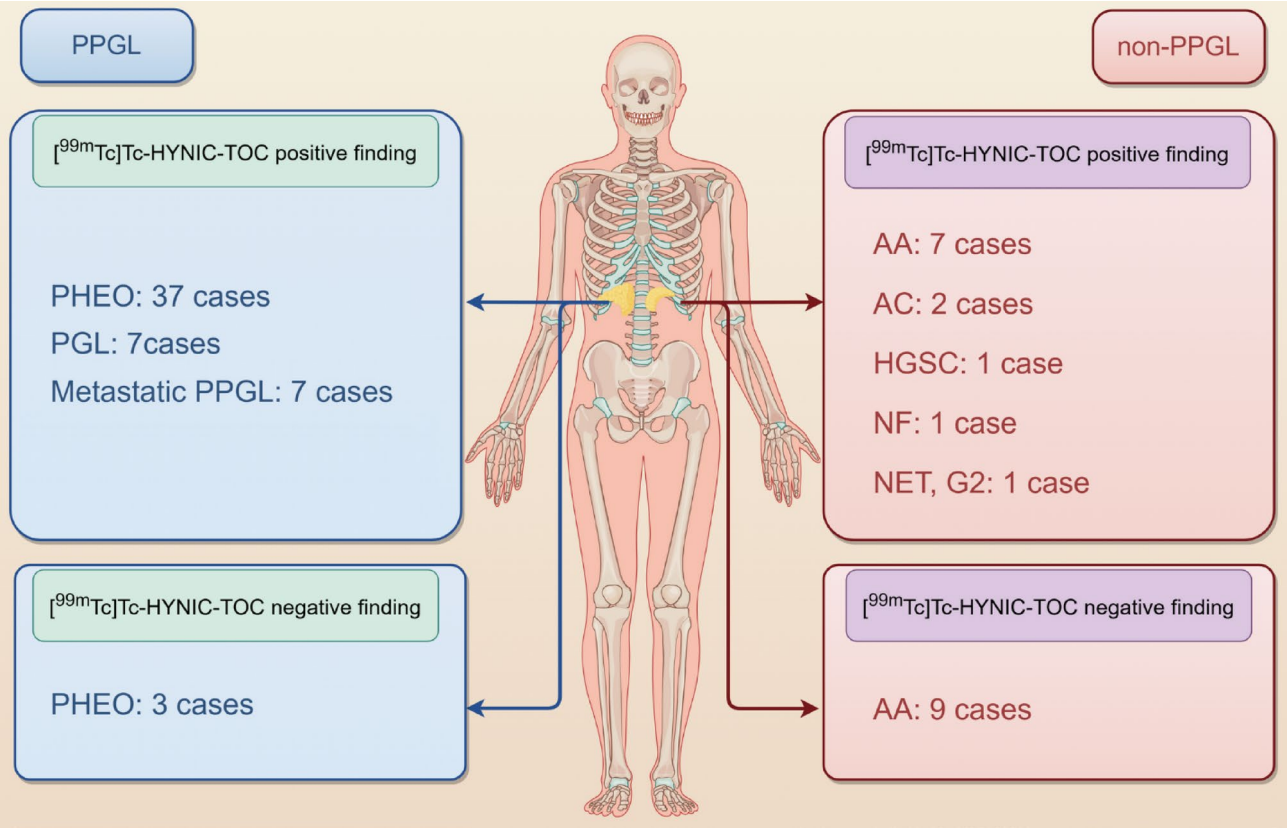

Fig. 3. Summary of [^{99m}Tc]Tc-HYNIC-TOC SPECT/CT finding in PPGL and non-PPGL.

[^{99m}Tc]Tc-HYNIC-TOC SPECT/CT	Histology		Index
	Positive, *n* (%)	Negative, *n* (%)	
Positive, n (%)	51 (68.0)	12 (16.0)	PPV = 80.9%
Negative, n (%)	3 (4.0)	9 (12.0)	NPV = 75.0%
Index	Se = 94.4%	Sp = 42.9%	Ac = 80.0%

Table 2. Diagnostic accuracy of [^{99m}Tc]Tc-HYNIC-TOC SPECT/CT for PPGLs. Se, sensitivity; Sp, specificity; PPV, positive predictive value; NPV, negative predictive value; Ac, Accuracy.

metanephrines) with SSTR imaging is essential, as these exhibit high sensitivity and specificity for PPGL diagnosis and could differentiate true PPGLs from SSTR-positive non-PPGL lesions.

Three PHEOs were missed by [^{99m}Tc]Tc-HYNIC-TOC SPECT/CT in our study. Analysis revealed that false-negative PHEOs were smaller than positive cases, with a median diameter of 3.30 cm (range: 0.9–3.6 cm) compared to 4.80 cm (range: 1.8–11.8 cm) in the positive group, though this difference was not statistically significant ($p = 0.10$), likely due to the small sample size ($n = 3$). The smallest missed lesion measured 0.9 cm, suggesting tumor size as a potential contributing factor. Several mechanisms may explain these false-negative results: insufficient radiotracer accumulation in smaller lesions due to lower absolute SSTR density, partial volume effects reducing detectability on SPECT imaging and inherently low SSTR expression in these specific tumors. The positive correlation between tumor size and tracer uptake intensity supports the hypothesis that smaller tumors with lower SSTR expression are more susceptible to false-negative results. Given the limited number of false-negative cases, these observations should be interpreted cautiously and warrant validation in larger cohorts.

Recently, there has been a shift towards exploring SSTR-targeted PET/CT imaging, which has shown promising outcomes. Gild et al.[23] demonstrated that [^{68}Ga]Ga-DOTATATE PET/CT offers high sensitivity (88% for PHEO and 100% for PGL) in preoperative assessments, advocating its use in suspected PPGL cases linked to hereditary syndromes or metastases. Similarly, Maurice et al.[10] compared [^{68}Ga]Ga-DOTA-TATE PET/CT with [^{123}I]I-MIBG SPECT, reporting a sensitivity of 80% for [^{68}Ga]Ga-DOTA-TATE and superior detection of lesions over [^{123}I]I-MIBG. Other studies, such as Jaiswal et al.[24] and Tan et al.[25] reported sensitivities exceeding 93% for [^{68}Ga]Ga-DOTATATE in PPGL detection. In contrast, our study found a sensitivity of 94.4% with [^{99m}Tc]

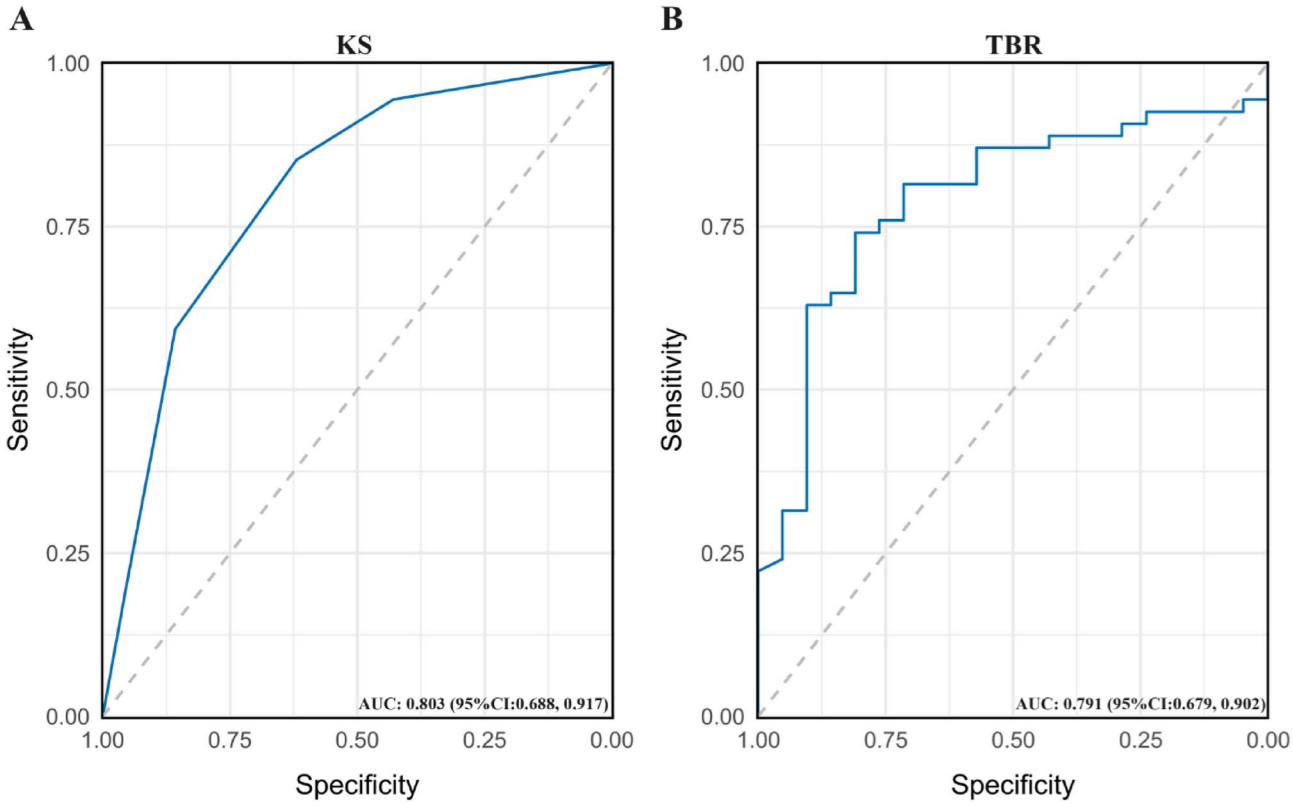

Fig. 4. ROC curve analysis of KS (**A**) and TBR (**B**) for diagnosing PPGLs on [^{99m}Tc]Tc-HYNIC-TOC SPECT/CT.

	Se	Sp	PPV	NPV	Ac
KS	85.2% (46/54)	61.9% (13/21)	85.2% (46/54)	61.9% (13/21)	78.7% (59/75)
TBR	74.1% (40/54)	81.0% (17/21)	90.9% (40/44)	54.8% (17/31)	76.0% (57/75)

Table 3. Sensitivity, specificity, positive predictive value, negative predictive value, and accuracy of KS and TBR for for diagnosing PPGL on [^{99m}Tc]Tc-HYNIC-TOC SPECT/CT. Se, sensitivity; Sp, specificity; PPV, positive predictive value; NPV, negative predictive value; Ac, Accuracy.

Tc-HYNIC-TOC SPECT/CT, surpassing the 80% reported by Maurice et al. but aligning closely with the higher sensitivities noted by others.

Moreover, SSTR-targeted imaging has consistently shown superior diagnostic performance in metastatic PPGL. In the present study, [^{99m}Tc]Tc-HYNIC-TOC SPECT/CT revealed positive findings consistent with metastatic involvement in all seven patients with metastatic disease, achieving a 100% per-patient detection rate for this subgroup. This observation aligns with prior research, such as Janssen et al.[26], who reported a lesion-based detection rate of 98.6% using [^{68}Ga]Ga-DOTATATE PET/CT in SDHB-related metastatic PPGL, significantly outperforming [^{18}F]F-FDG (85.8%), [^{18}F]F-FDOPA (61.4%), [^{18}F]F-FDA (51.9%), and CT/MRI (84.8%). In sporadic metastatic PPGL, Janssen et al.[27] documented a 97.6% lesion-based detection rate with [^{68}Ga]Ga-DOTATATE PET/CT, compared to 49.2% for [^{18}F]F-FDG, 74.8% for [^{18}F]F-FDOPA, 77.7% for [^{18}F]F-FDA, and 81.6% for CT/MRI. Similarly, Jha et al.[28] reported a 93.5% per-lesion detection rate in pediatric SDHx-related PPGL using [^{68}Ga]Ga-DOTATATE PET/CT, surpassing [^{18}F]F-FDG PET/CT (79.4%) and CT/MRI (73.8%). Jha et al.[29] further emphasized its utility in detecting spinal bone metastases in PPGL, achieving a 98.7% per-lesion detection rate, compared to 72.0% for [^{18}F]F-FDG PET/CT and 80.6% for spinal MRI. Patel et al.[30] noted an 88.6% lesion-based detection rate with [^{68}Ga]Ga-DOTATATE in SDHA-related metastatic PPGL, although [^{18}F]F-FDG identified additional lesions in specific regions, suggesting potential complementary roles for these modalities. Notably, across these various cohorts, the per-patient detection rates for [^{68}Ga]Ga-DOTATATE were generally 100% in metastatic patients, with the exception of SDHA-related cases. Collectively, these studies underscore the exceptional diagnostic accuracy of SSTR-targeted imaging, particularly [^{68}Ga]Ga-DOTATATE PET/CT, positioning it as the preferred imaging modality for the evaluation of metastatic PPGL.

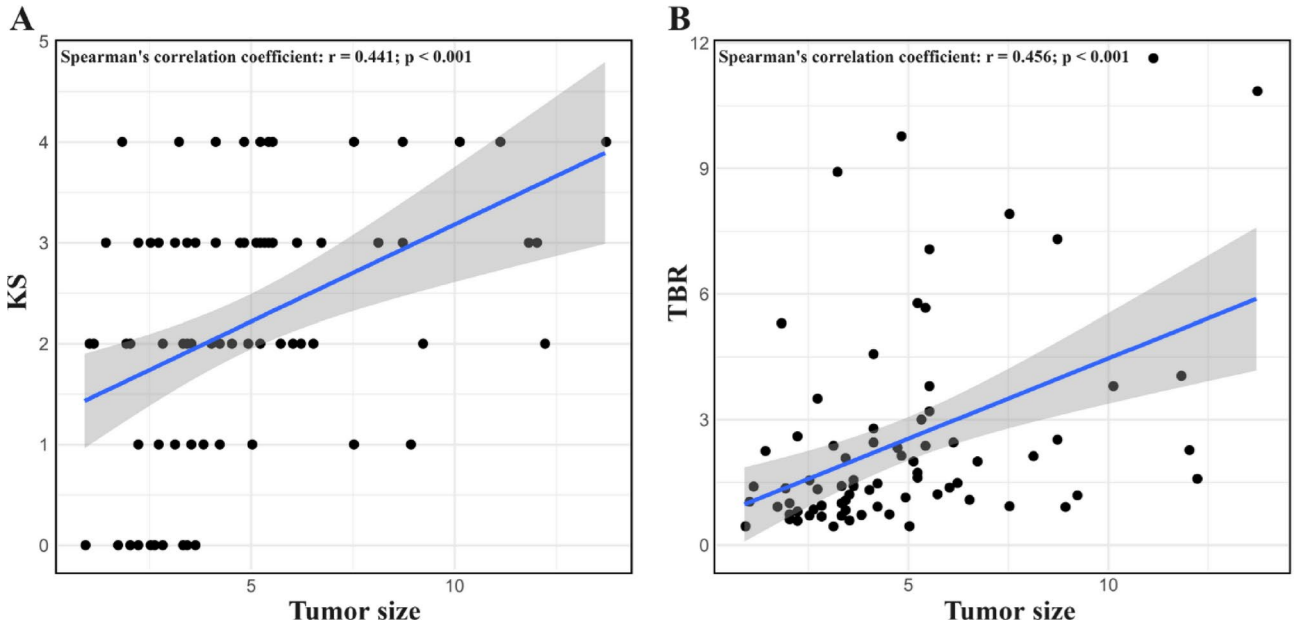

Fig. 5. Dot plots showing moderate positive correlations between tumor size and KS (**A**) and TBR (**B**).

		PHEO	PGL		Non-metastatic PPGL	Metastatic PPGL	
Variable	**Overall, *N* = 54[1]**	***N* = 46 (85%)[1]**	***N* = 8 (15%)[1]**	**p-value[2]**	***N* = 47 (87%)[1]**	***N* = 7 (13%)[1]**	**p-value[2]**
Age	50.50 [36.00, 58.00]	50.50 [36.00, 56.75]	53.00 [36.75, 64.00]	0.584	50.00 [35.50, 58.50]	53.00 [43.00, 54.50]	0.887
Sex				0.706			0.047
Female	28 (51.85%)	23 (50.00%)	5 (62.50%)		27 (57.45%)	1 (14.29%)	
Male	26 (48.15%)	23 (50.00%)	3 (37.50%)		20 (42.55%)	6 (85.71%)	
Tumor size (cm)	4.85 [3.43, 6.08]	4.75 [3.33, 6.18]	5.10 [4.80, 5.23]	0.817	4.80 [3.35, 5.50]	8.70 [5.05, 10.70]	0.058
KS				0.491			0.750
0	3 (5.56%)	3 (6.52%)	0 (0.00%)		3 (6.38%)	0 (0.00%)	
1	5 (9.26%)	4 (8.70%)	1 (12.50%)		5 (10.64%)	0 (0.00%)	
2	14 (25.93%)	10 (21.74%)	4 (50.00%)		11 (23.40%)	3 (42.86%)	
3	21 (38.89%)	19 (41.30%)	2 (25.00%)		19 (40.43%)	2 (28.57%)	
4	11 (20.37%)	10 (21.74%)	1 (12.50%)		9 (19.15%)	2 (28.57%)	
TBR	2.10 [1.33, 3.43]	2.19 [1.38, 3.73]	1.29 [1.04, 2.05]	0.141	2.08 [1.28, 3.35]	2.25 [1.45, 4.88]	0.562

Table 4. Comparison between PHEO and PGL, and between non-metastatic and metastatic PPGL. [1]Mean (SD); Median [IQR]; n (%). [2]Wilcoxon rank sum test; Fisher's exact test. PHEO, pheochromocytoma; PGL, paraganglioma; KS, Krenning score; TBR, ratio between the maximal counts within the lesion and the mean counts within the liver.

Furthermore, it is important to consider that other radiotracers, notably [^{18}F]F-FDOPA, can exhibit superior performance for specific PPGL subtypes, particularly sporadic PHEOs. A prospective intraindividual comparison by Jha et al.[31] demonstrated that [^{18}F]F-FDOPA PET/CT achieved a 100% positivity rate in sporadic primary PHEOs, with the highest conspicuity score (5.0 ± 0.0) and lesion-to-liver SUVmax ratio (10.5). This was in contrast to [^{68}Ga]Ga-DOTATATE PET/CT, which showed a 78.6% positivity rate and a lower lesion-to-liver SUVmax ratio (3.0-4.2) in the same cohort. Similarly, while Archier et al.[32] reported comparable overall patient-based sensitivities for [^{68}Ga]Ga-DOTATATE and [^{18}F]F-FDOPA PET/CT (93% vs. 97%, respectively) across various PPGLs, their findings suggested that [^{18}F]F-FDOPA PET/CT may be superior for detecting PHEOs. Conversely, [^{68}Ga]Ga-DOTATATE PET/CT excelled in identifying head and neck PGLs, especially those related to SDHD mutations. These studies underscore that while SSTR-targeted imaging offers excellent overall diagnostic value, [^{18}F]F-FDOPA PET/CT is often the preferred modality for sporadic PHEOs. Consequently, PHEOs yielding negative or equivocal results with SSTR-targeted agents, such as the [^{99m}Tc]Tc-HYNIC-TOC SPECT/CT utilized in our study, are prime candidates for subsequent [^{18}F]F-FDOPA PET/CT imaging.

In this study, we employed both visual and quantitative methods to analyze [^{99m}Tc]Tc-HYNIC-TOC SPECT/CT images. Liver uptake was utilized as an internal reference for KS and TBR, potentially mitigating interference from radiopharmaceutical dosage. The KS is widely used visually and conveniently to interpret [^{68}Ga]Ga-DOTA-

TATE PET/CT images, aiding in the selection of patients suitable for targeted SSTR radioligand therapy[33]. However, its application for PPGL diagnosis using [^{99m}Tc]Tc-HYNIC-TOC SPECT/CT images has not been validated. For the first time, visual KS was utilized to assess [^{99m}Tc]Tc-HYNIC-TOC uptake in PPGL patients. In our study, PPGLs demonstrated higher KS and TBR values compared to non-PPGLs (both $P < 0.001$), reinforcing the high expression of SSTR in PPGLs. Furthermore, our study found a moderate positive correlation between tumor size and the uptake of [^{99m}Tc]Tc-HYNIC-TOC. This demonstration of SSTR expression in tumors may offer opportunities for the treatment of these tumors with peptide receptor radionuclide therapy.

Despite significant differences in KS and TBR between PPGL and non-PPGL, there was considerable overlap between these values. Semi-quantitative analysis of SSTR expression in tumor specimens from PPGL patients by Leijon et al.[34] and Shen et al.[35] indicated that SSTR expression varied from negative to strong within these tumors. In addition, our study also found that approximately 57.1% (12/21) of non-PPGL tumors exhibited uptake of [^{99m}Tc]Tc-HYNIC-TOC, ranging from weak to moderate. Considering the varying levels of SSTR expression in both PPGL and non-PPGL tumors, we conducted ROC analysis to determine the optimal threshold for diagnosing PPGL. The optimal cut-off values for KS and TBR in this study were 2 and 1.356, respectively, aligning with the clinical standard of defining SSTR positivity as lesion uptake greater than that of normal liver[33]. Sensitivity, specificity, and accuracy of KS and TBR were 85.2%, 61.9%, and 78.7%, and 74.1%, 81.0%, and 76.0%, respectively. These results indicate that KS has slightly higher diagnostic accuracy than TBR. However, it should be noted that the sensitivity and specificity of these cutoff points are limited. Therefore, the proposed thresholds require further validation in clinical practice.

Furthermore, we conducted separate analyses of PHEO and PGL and observed no significant difference in the uptake of [^{99m}Tc]Tc-HYNIC-TOC between the two groups. This finding contrasts with the results of Ma et al.[36]who reported a significantly higher uptake of [^{68}Ga]Ga-DOTATATE in PHEO compared to PGL. The discrepancy may be attributed to the relatively small number of PGL cases in our study, with only seven cases available for analysis. In metastatic PPGL, an increased expression of SSTR receptors is typically observed[37,38]. Previous studies on [^{111}In]In-Octreotide have indicated a higher sensitivity in detecting metastatic PHEO compared to non-metastatic PHEO[39]. In our study, we found no significant differences in KS and TBR between metastatic and non-metastatic PPGL. This may be partially due to the larger tumor volume in metastatic PPGL cases, which could lead to a decreased SSTR density and consequently a reduced uptake of [^{99m}Tc]Tc-HYNIC-TOC.

This study has several limitations. First, the retrospective design introduces selection bias, as 74% of patients (213/288) were excluded due to absent pathological or follow-up data. This substantial exclusion rate may have led to overestimation of diagnostic performance, particularly sensitivity, since excluded cases potentially included patients with ambiguous imaging findings less likely to receive definitive histopathological confirmation. Additionally, patients who underwent surgical resection or biopsy may represent a subset with more clinically evident disease, potentially inflating diagnostic accuracy estimates. These factors limit the generalizability of our findings to broader patient populations. Second, the small sample sizes in key subgroups represent a significant limitation. With only 8 patients with PGLs and 7 with metastatic PPGLs, statistical power for meaningful subgroup analyses was substantially restricted, limiting our ability to draw definitive conclusions about diagnostic performance in these clinically important populations. These subgroup findings should therefore be interpreted with considerable caution as preliminary observations. Future multicenter studies with larger patient cohorts are essential to validate our findings, particularly for PGLs and metastatic disease, where diagnostic accuracy has critical implications for patient management. Third, although genetic testing is recommended for all PPGL patients, high cost and limited insurance coverage in China resulted in unknown genetic status for most patients. This represents a significant limitation, as genetic stratification profoundly influences SSTR expression patterns and imaging performance. Among the 54 diagnosed PPGL patients, SDHB immunohistochemistry revealed loss of expression in three cases, suggesting possible SDHx germline mutations. The absence of comprehensive genetic data limits our ability to stratify diagnostic performance based on genetic subtypes, which is crucial for understanding the clinical utility of [^{99m}Tc]Tc-HYNIC-TOC SPECT/CT. Additionally, tumor SSTR expression profiles were not available, preventing correlation between tracer uptake intensity and actual receptor density. Fourth, a major limitation is the absence of direct head-to-head comparison with established imaging modalities in the same patient cohort. We did not compare [^{99m}Tc]Tc-HYNIC-TOC SPECT/CT with [^{68}Ga]Ga-DOTATATE PET/CT, [^{18}F]F-FDOPA PET/CT, or [^{123}I]I-MIBG scintigraphy, which are considered reference standards for PPGL imaging. This prevents direct assessment of relative diagnostic performance and clinical utility. Finally, as a single-center study, quantitative results may be influenced by specific equipment and imaging techniques, potentially limiting generalizability. Therefore, future multicenter prospective studies with head-to-head comparisons are essential to address these critical limitations, enable robust statistical comparison of diagnostic performance metrics, and determine the appropriate clinical positioning of [^{99m}Tc]Tc-HYNIC-TOC SPECT/CT in PPGL evaluation.

Conclusion

In conclusion, our study demonstrated that [^{99m}Tc]Tc-HYNIC-TOC SPECT/CT shows promise as a diagnostic tool for PPGL, effectively differentiating between PPGL and non-PPGL tumors and identifying metastatic cases. However, the low specificity, retrospective nature, and small subgroup sizes necessitate cautious interpretation. While PET-based tracers offer superior performance, [^{99m}Tc]Tc-HYNIC-TOC SPECT/CT represents a cost-effective alternative for evaluating PPGLs, especially where genetic testing is unavailable and PET/CT access is limited. This modality effectively bridges the diagnostic gap in healthcare systems with constrained resources while maintaining acceptable diagnostic accuracy.

Data availability

The data generated and analyzed in this study are available from the corresponding author upon reasonable request.

Received: 1 November 2024; Accepted: 21 July 2025
Published online: 28 July 2025

References

1. Lenders, J. W. M. et al. Pheochromocytoma and paraganglioma: an endocrine society clinical practice guideline. *J. Clin. Endocrinol. Metabolism*. **99**, 1915–1942 (2014).
2. Lenders, J. W. M. et al. Biochemical Diagnosis of Pheochromocytoma. *JAMA*. **287**, (2002).
3. Constantinescu, G. et al. Silent pheochromocytoma and paraganglioma: systematic review and proposed definitions for standardized terminology. *Frontiers Endocrinology* **13**, (2022).
4. He, Q. et al. Head-to-head comparison between [68Ga]Ga-DOTA-NOC and [18F]DOPA PET/CT in a diverse cohort of patients with pheochromocytomas and paragangliomas. *Eur. J. Nucl. Med. Mol. Imaging*. **51**, 1989–2001 (2024).
5. Sung, C. et al. A prospective comparative study of 18F-FDOPA PET/CT versus 123I-MIBG scintigraphy with SPECT/CT for the diagnosis of pheochromocytoma and paraganglioma. *Clin. Nucl. Med*. **49**, 27–36 (2023).
6. Bombardieri, E. et al. 131I/123I-metaiodobenzylguanidine (mIBG) scintigraphy: procedure guidelines for tumour imaging. *Eur. J. Nucl. Med. Mol. Imaging*. **37**, 2436–2446 (2010).
7. Feggi, L. et al. Pitfalls in scintigraphic detection of neuroendocrine tumours. *Eur. J. Nucl. Med.* **19**, 214–218 (1992).
8. Taïeb, D. et al. European association of nuclear medicine practice guideline/society of nuclear medicine and molecular imaging procedure standard 2019 for radionuclide imaging of Phaeochromocytoma and paraganglioma. *Eur. J. Nucl. Med. Mol. Imaging*. **46**, 2112–2137 (2019).
9. Naswa, N. et al. Prospective evaluation of ^{68}Ga-DOTA-NOC PET-CT in Phaeochromocytoma and paraganglioma: preliminary results from a single centre study. *Eur. Radiol.* **22**, 710–719 (2012).
10. Maurice, J. B. et al. A comparison of the performance of ^{68}Ga-DOTATATE PET/CT and ^{123}I-MIBG SPECT in the diagnosis and follow-up of Phaeochromocytoma and paraganglioma. *Eur. J. Nucl. Med. Mol. Imaging*. **39**, 1266–1270 (2012).
11. Janssen, I. et al. Functional imaging signature of patients presenting with polycythemia/paraganglioma syndromes. *J. Nucl. Med.* **58**, 1236–1242 (2017).
12. Taïeb, D. et al. 18F-FDOPA PET/CT imaging of MAX-related pheochromocytoma. *J. Clin. Endocrinol. Metab.* **103**, 1574–1582 (2018).
13. Jha, A. et al. Sporadic primary pheochromocytoma: A prospective intraindividual comparison of six imaging tests (CT, MRI, and PET/CT using 68Ga-DOTATATE, FDG, 18F-FDOPA, and 18F-FDA). *AJR Am. J. Roentgenol.* **218**, 342–350 (2021).
14. Archier, A. et al. Prospective comparison of (68)Ga-DOTATATE and (18)F-FDOPA PET/CT in patients with various pheochromocytomas and paragangliomas with emphasis on sporadic cases. *Eur. J. Nucl. Med. Mol. Imaging*. **43**, 1248–1257 (2015).
15. Liepe, K. & Becker, A. 99mTc-Hynic-TOC imaging in the diagnostic of neuroendocrine tumors. *World J. Nucl. Med.* **17**, 151–156 (2018).
16. Li, B. et al. [99mTc]Tc-HYNIC-ALUG SPECT/CT in the initial staging of 227 consecutive patients with newly diagnosed prostate cancer: a 5-year monocentric retrospective study. *Front. Endocrinol.* **15**, 1326858 (2024).
17. Li, B. et al. Diagnostic accuracy of 99mTc-HYNIC-TOC SPECT/CT for detecting osteomalacia-associated tumors. *Front. Oncol.* **13**, 1228575 (2023).
18. Gabriel, M. et al. An intrapatient comparison of 99mTc-EDDA/HYNIC-TOC with 111In-DTPA-octreotide for diagnosis of somatostatin receptor-expressing tumors. *J. Nucl. Med.* **44**, 708–716 (2003).
19. Ilias, I. et al. Comparison of 6-18F-fluorodopamine PET with 123I-metaiodobenzylguanidine and 111in-pentetreotide scintigraphy in localization of nonmetastatic and metastatic pheochromocytoma. *J. Nucl. Med.* **49**, 1613–1619 (2008).
20. King, K. S. et al. Functional imaging of SDHx-related head and neck paragangliomas: comparison of 18F-fluorodihydroxyphenylalanine, 18F-fluorodopamine, 18F-fluoro-2-deoxy-D-glucose PET, 123I-metaiodobenzylguanidine scintigraphy, and 111In-pentetreotide scintigraphy. *J. Clin. Endocrinol. Metab.* **96**, 2779–2785 (2011).
21. Decristoforo, C., Melendez-Alafort, L., Sosabowski, J. K. & Mather, S. J. 99mTc-HYNIC-[Tyr3]-octreotide for imaging somatostatin-receptor-positive tumors: preclinical evaluation and comparison with 111In-octreotide. *J. Nucl. Med.* **41**, 1114–1119 (2000).
22. Ueberberg, B. et al. Differential expression of the human somatostatin receptor subtypes sst1 to sst5 in various adrenal tumors and normal adrenal gland. *Horm. Metab. Res.* **37**, 722–728 (2005).
23. Gild, M. L. et al. Role of DOTATATE-PET/CT in preoperative assessment of Phaeochromocytoma and paragangliomas. *Clin. Endocrinol. (Oxf)*. **89**, 139–147 (2018).
24. Jaiswal, S. K. et al. The utility of 68Ga-DOTATATE PET/CT in localizing primary/metastatic pheochromocytoma and paraganglioma in children and adolescents - a single-center experience. *J. Pediatr. Endocrinol. Metab.* **34**, 109–119 (2021).
25. Tan, T. H., Hussein, Z., Saad, F. F. A. & Shuaib, I. L. Diagnostic performance of (68)Ga-DOTATATE PET/CT, (18)F-FDG PET/CT and (131)I-MIBG scintigraphy in mapping metastatic pheochromocytoma and paraganglioma. *Nucl. Med. Mol. Imaging* (2010). **49**, 143–151 (2015).
26. Janssen, I. et al. Superiority of [68Ga]-DOTATATE PET/CT to other functional imaging modalities in the localization of SDHB-associated metastatic pheochromocytoma and paraganglioma. *Clin. Cancer Res.* **21**, 3888–3895 (2015).
27. Janssen, I. et al. PET/CT comparing (68)Ga-DOTATATE and other radiopharmaceuticals and in comparison with CT/MRI for the localization of sporadic metastatic pheochromocytoma and paraganglioma. *Eur. J. Nucl. Med. Mol. Imaging*. **43**, 1784–1791 (2016).
28. Jha, A. et al. Superiority of 68Ga-DOTATATE over 18F-FDG and anatomic imaging in the detection of succinate dehydrogenase mutation (SDHx)-related pheochromocytoma and paraganglioma in the pediatric population. *Eur. J. Nucl. Med. Mol. Imaging*. **45**, 787–797 (2018).
29. Jha, A. et al. Diagnostic performance of [68Ga]DOTATATE PET/CT, [18F]FDG PET/CT, MRI of the spine, and whole-body diagnostic CT and MRI in the detection of spinal bone metastases associated with pheochromocytoma and paraganglioma. *Eur. Radiol.* **34**, 6488–6498 (2024).
30. Patel, M. et al. Performances of functional and anatomic imaging modalities in succinate dehydrogenase A-Related metastatic pheochromocytoma and paraganglioma. *Cancers (Basel)* **14**, (2022).
31. Jha, A. et al. Sporadic primary pheochromocytoma: A prospective intraindividual comparison of six imaging tests (CT, MRI, and PET/CT using 68Ga-DOTATATE, FDG, 18F-FDOPA, and 18F-FDA). *AJR Am. J. Roentgenol.* **218**, 342–350 (2022).
32. Archier, A. et al. Prospective comparison of (68)Ga-DOTATATE and (18)F-FDOPA PET/CT in patients with various pheochromocytomas and paragangliomas with emphasis on sporadic cases. *Eur. J. Nucl. Med. Mol. Imaging*. **43**, 1248–1257 (2016).
33. Hope, T. A., Calais, J., Zhang, L., Dieckmann, W. & Millo, C. 111In-pentetreotide scintigraphy versus 68Ga-DOTATATE PET: impact on Krenning scores and effect of tumor burden. *J. Nucl. Med.* **60**, 1266–1269 (2019).
34. Leijon, H. et al. Variable somatostatin receptor subtype expression in 151 primary pheochromocytomas and paragangliomas. *Hum. Pathol.* **86**, 66–75 (2019).

35. Shen, Y. et al. Somatostatin receptor subtype 2A expression and genetics in 184 paragangliomas: a single center retrospective observational study. *Endocrine* https://doi.org/10.1007/s12020-023-03595-1 (2024).
36. Ma, G. et al. Quantitative analysis of 68Ga-DOTA(0)-Tyr(3)-octreotate positron emission tomography/computed tomography imaging for the differential diagnosis of primary pheochromocytoma and paraganglioma. *Quant. Imaging Med. Surg.* **12**, 2427–2440 (2022).
37. Fischer, A. et al. Metastatic pheochromocytoma and paraganglioma: somatostatin receptor 2 expression, genetics, and therapeutic responses. *J. Clin. Endocrinol. Metab.* **108**, 2676–2685 (2023).
38. Crona, J., Taïeb, D. & Pacak, K. New perspectives on pheochromocytoma and paraganglioma: toward a molecular classification. *Endocr. Rev.* **38**, 489–515 (2017).
39. van der Harst, E. et al. [123I]Metaiodobenzylguanidine and[111In]Octreotide uptake in benign and malignant Pheochromocytomas1. *J. Clin. Endocrinol. Metabolism*. **86**, 685–693 (2001).

Acknowledgements

We extend our gratitude to Haizhou Sun and Xiaofei Li for their valuable contributions to the acquisition and processing of SPECT/CT images in the Department of Nuclear Medicine at Henan Provincial People's Hospital & Zhengzhou University People's Hospital. We also acknowledge the Home for Researchers editorial team (www.home-for-researchers.com) for their assistance with language editing services and Figdraw for their assistance in the creation of Fig. 3.

Author contributions

YG, BL, and HL designed the present study. BL, XD, HL and XW collected and analyzed the data. JZ and MT analyzed the data. BL, XD and YG drafted the manuscript. YG and BL can authenticate all raw data. All authors reviewed and approved the final manuscript.

Funding

This study was supported by the Henan Provincial Medical Science and Technology Project (grant no. LHGJ20240030 and SBGJ202102015), and the Henan Key Laboratory of Molecular Nuclear Medicine and Translational Medicine (grant no. 2020-27-4).

Declarations

Competing interests

The authors declare no competing interests.

Ethical approval and informed consent

This study was approved by the Institutional Review Boards (IRB) of Henan Provincial People's Hospital & Zhengzhou University People's Hospital (Approval No. 24-0510). This study is retrospective in nature, and the requirement for informed consent was waived by the IRB of Henan Provincial People's Hospital & Zhengzhou University People's Hospital in accordance with the relevant guidelines and regulations.

Additional information

Correspondence and requests for materials should be addressed to H.L., X.W. or Y.G.